Int. J. Electrochem. Sci., 8 **(2013)** 4283 - 4304

International Journal of
ELECTROCHEMICAL
SCIENCE
www.electrochemsci.org

Kinetics of Electrochemical Reduction of NAD^+ on a Glassy Carbon Electrode

Irshad Ali and Sasha Omanovic[*]

Department of Chemical Engineering, McGill University, 3610 University Street, Montreal, Quebec, Canada, H3A 0C5
[*]E-mail: sasha.omanovic@mcgill.ca

Received: 5 January 2013 / *Accepted:* 28 January 2013 / *Published:* 1 March 2013

The kinetics of reduction of nicotinamide adenine dinucleotide, NAD^+, was investigated on glassy carbon (GC) electrode at various temperatures, electrode potentials and NAD^+ concentrations using electrochemical methods of linear polarization voltammetry, differential pulse voltammetry and electrochemical impedance spectroscopy. It was shown that under the experimental conditions employed, the NAD^+ reduction reaction is under diffusion control, is irreversible (requires overpotential of more than -550 mV), and is of pseudo-first order with respect to NAD^+. The reduction process involves the exchange of 1.54 or 1.62 electrons, depending on reduction potential. This indicates that 54 or 62 mol% of NADH is produced, respectively, while the remaining quantity is NAD_2. The kinetics of NAD^+ reduction at a *formal* potential of the NAD^+/NADH couple was found to be rather slow, and only moderately temperature dependent: the apparent formal heterogeneous electron-transfer rate constant is in the order of 10^{-14} cm s^{-1}, and the apparent formal Gibbs energy of activation is 53.1 kJ mol^{-1}.

Keywords: NAD^+ electrochemical reduction kinetics; Glassy carbon; Linear voltammetry; Differential pulse voltammetry; Electrochemical impedance spectroscopy

1. INTRODUCTION

Nicotinamide adenine dinucleotide NAD(H) is a coenzyme of great importance in a large number of biochemical processes, in which it serves as an electron and hydrogen shuttle [1-3]. Consequently, NAD(H) is found in two redox forms: oxidized NAD^+ and reduced NADH (the only enzymatically-active isomer of the latter is 1,4-NADH). NAD(H) is also used in medicine for treatment of certain diseases, such as Alzheimer's and Parkinson's, in pharmacology, biotechnology, biosensors development, and for the synthesis of new high-value-added compounds such as pharmaceuticals, food additives, perfumes, insecticides and pesticides [4-12].

Since a stoichiometric amount of NAD(H) is consumed in these processes and because of its high price, especially that of the reduced form, 1,4-NADH (ca. $1,186,900/kg [13], but the actual price depends on its form), the industrial use of the coenzyme is rather limited. Thus, there is a great interest to develop NAD(H) regeneration methods, which would enable re-use of NAD(H) initially introduced into a (bio)reactor.

With respect to the regeneration of a reduced form of the coenzyme NADH, several regeneration methods have been developed, including enzymatic, electrochemical, chemical, photochemical and biological [14]. However, electrochemical methods are of particular interest due to their potential low cost, no need to add a reducing agent at stoichiometric quantities, and due to relatively simple product isolation. A problem that arises in direct regeneration of NADH on unmodified electrodes is the formation of an enzymatically-inactive NAD_2 dimer, as shown in Scheme 1.

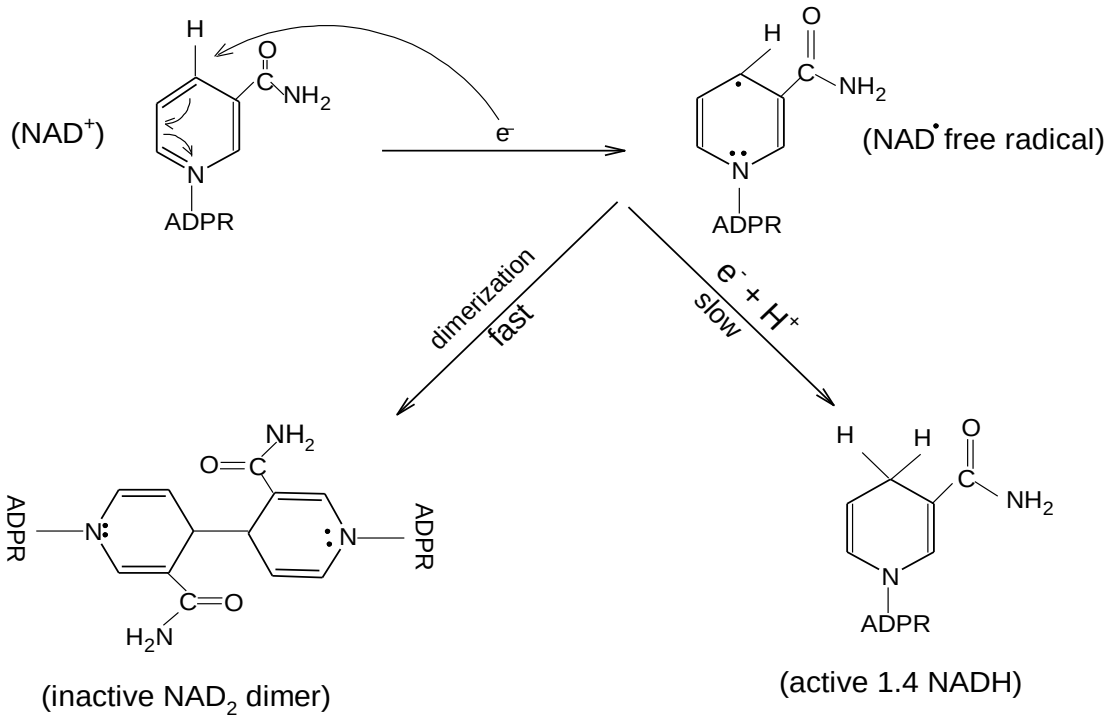

Scheme 1. Reduction of NAD^+ to NAD_2 and enzymatically-active 1,4-NADH. ADPR= adenosine diphosphoribose.

In the first step, reduction of NAD^+ results in the formation of an NAD-free radical. In the second step, two reaction pathways are possible; (i) two neighboring free radicals can combine in a very fast dimerization reaction to form enzymatically-inactive NAD_2, or (ii) the radical can be protonated and further reduced to form enzymatically-active 1,4 NADH. Unfortunately, the literature demonstrates that on bare (unmodified) electrodes the kinetics of path (ii) is significantly slower than that of path (i), and thus the major product of NAD^+ reduction on these electrodes is the enzymatically-inactive dimer. This formation of the dimer reduces the yield of enzymatically-active NADH that could be produced (regenerated). For example, reduction of NAD^+ on a gold-amalgam unmodified electrode gave only ca. 10% enzymatically-active 1,4-NADH, while the yield in active NADH

increased to 50% when an unmodified platinum electrode was used [15]. However, our recent work on the regeneration of 1,4-NADH on a bare glassy-carbon (GC) electrode and Pt and Ni modified glassy carbon electrode demonstrated that the amount of active 1,4-NADH regenerated strongly depends on the applied regeneration potential, the fact that seems not to have been investigated by other research group [16, 17].

In order to increase the yield of active NADH regenerated, many research groups [3, 15, 18-21] including ours [17, 22-25], have developed 'surface-modified' electrodes. Depending on the electrode used, the corresponding yield of active 1,4-NADH regenerated ranged from 75% on a cholesterol-modified gold-amalgam electrode [15] to 98% on Pt and Ni-modified glassy-carbon electrode [17].

To develop electrochemical systems capable of regenerating 1,4-NADH at high yields, it is important to obtain information on the fundamental electrochemical behavior of NAD^+ at electrode surfaces, namely on the NAD^+ reduction mechanisms, kinetics, mass-transport, adsorption and electrode surface conformation of the molecule. Many research groups have indeed studied some of these aspects, mostly on bare (non-modified) metallic electrodes, such as mercury [26-35] and a variety of carbon materials [36]. Our laboratory has also investigated the NAD^+ reduction reaction on several electrode surfaces, including gold [24], Pt-modified gold [23], copper [23], and Ru, Pt and Ni-modified glassy carbon [17, 25].

This manuscript presents first part of our results on the interaction of NAD^+ with a glassy carbon surface, *i.e.* on the kinetics of NAD^+ reduction. Glassy carbon was chosen as electrode since it offers high hydrogen reduction overpotential (thus minimizing the interference of this reaction with the NAD^+ reduction reaction), low porosity, and relatively good electrical conductivity [37]. In addition, GC is a good candidate material for industrial applications, due to its relatively low cost and stability.

It will be show that under the experimental conditions employed, the NAD^+ reduction reaction is under diffusion control, is irreversible and is of pseudo-first order with respect to NAD^+. The kinetics of reduction of NAD^+ on GC at a *formal* potential of the NAD^+/NADH couple (-0.885 V) is rather slow, and only moderately temperature dependent.

2. MATERIALS AND METHODS

NAD^+ reduction kinetics on a glassy carbon electrode was studied in 0.1 M $NaClO_4$ (HPLC grade, Fisher Scientific S490, pH = 5.8) at various temperatures (295 to 331 K), electrode potentials (-1.1 to –1.5 V) and NAD^+ concentrations (1 to 5 mM). NAD^+ solutions were prepared by dissolving a proper amount of β-NAD^+ (sodium salt, purity 98%, Sigma N0632) in supporting electrolyte. All chemicals were used as received, without further purification. Aqueous solutions were prepared using deionized water of resistivity 18.2 MΩ cm.

Electrochemical measurements were carried out in a two-compartment three-electrode batch electrochemical cell connected to a potentiostat/galvanostat/frequency response analyzer. The counter electrode was a graphite rod, which was, prior to each use, sonicated for 30 minutes in ethanol, followed by thorough rinsing with water. During measurements, the counter electrode was separated from the working and reference electrodes by a glass frit, in order to prevent oxygen evolved on it to

diffuse to the working electrode and get reduced, thus interfering with the NAD^+ reduction reaction. A mercury/mercurous sulphate electrode (MSE; +0.642 V vs. SHE) was used as a reference electrode, and all the potentials in this paper are referred to MSE. A glassy carbon (GC) electrode (5 mm in diameter) was used as a working electrode. Before each measurement, the surface of the GC electrode was carefully wet-polished with polishing paper (grid 1200/4000) until a mirror finish was obtained, followed by degreasing with ethanol and sonication for 5 min in ethanol in order to remove polishing residues. To ensure the clean surface, electrochemical pretreatment of GC was carried out in 0.5 M H_2SO_4 by cyclic potentiodynamic polarization between -1.5 V and 1.1 V at scan rate of 100 mV s^{-1}, for 50 cycles. This resulted in a stable/reproducible cyclic voltammetry (CV) profile confirming a clean GC surface. $K_4Fe(CN)_6 \times 3H_2O$ was used to determine the real electrochemically-active surface area of the GC electrode following the procedure published in the literature [38]. The area was calculated to be 0.206 cm^2. Therefore, in this study all the reported values are referred to the electrochemically-active surface area of the electrode, if not otherwise stated.

In order to maintain an oxygen-free electrolyte, argon (99.998% pure) was purged through the electrolyte prior electrochemical measurements for 30 minutes. After oxygen removal the bubbler was pulled out of the electrolyte surface. However, the oxygen-free electrolyte and the inert atmosphere above the electrolyte were maintained by saturating the cell space above the electrolyte with argon. All the measurements were made in a quiescent solution.

For concentration-dependent experiments, the stock NAD^+ solution was prepared in a separate container using the supporting electrolyte. Before measurements in a NAD^+-containing solution, the background response of the electrode was recorded in 0.1 M $NaClO_4$. Aliquots of NAD^+ were then added to the electrochemical cell and the electrochemical measurements were repeated for each aliquot.

Electrochemical techniques of linear polarization voltammetry (LV), differential pulse voltammetry (DPV) and electrochemical impedance spectroscopy (EIS) were employed using an Ecochemie Autolab potentiostat/galvanostat/frequency response analyzer PGSTAT30/FRA2, controlled by the GPES/FRA v.4.9.5 software.

3. RESULTS AND DISCUSSION

3.1. Linear polarization voltammetry

LV measurements were first performed in order to obtain the information on the potential region of NAD^+ reduction and initial information on the NAD^+ reduction kinetics. Fig. 1 shows the scan-dependent LVs recorded in the absence (curve 1, control curve) and presence (curves 2-6) of NAD^+ in the electrolyte. The control curve shows a typical behavior of a GC electrode, characterized by a wide double layer region (positive of ca.-1.5 V) and the beginning of a hydrogen reduction region (negative of ca. –1.5 V).

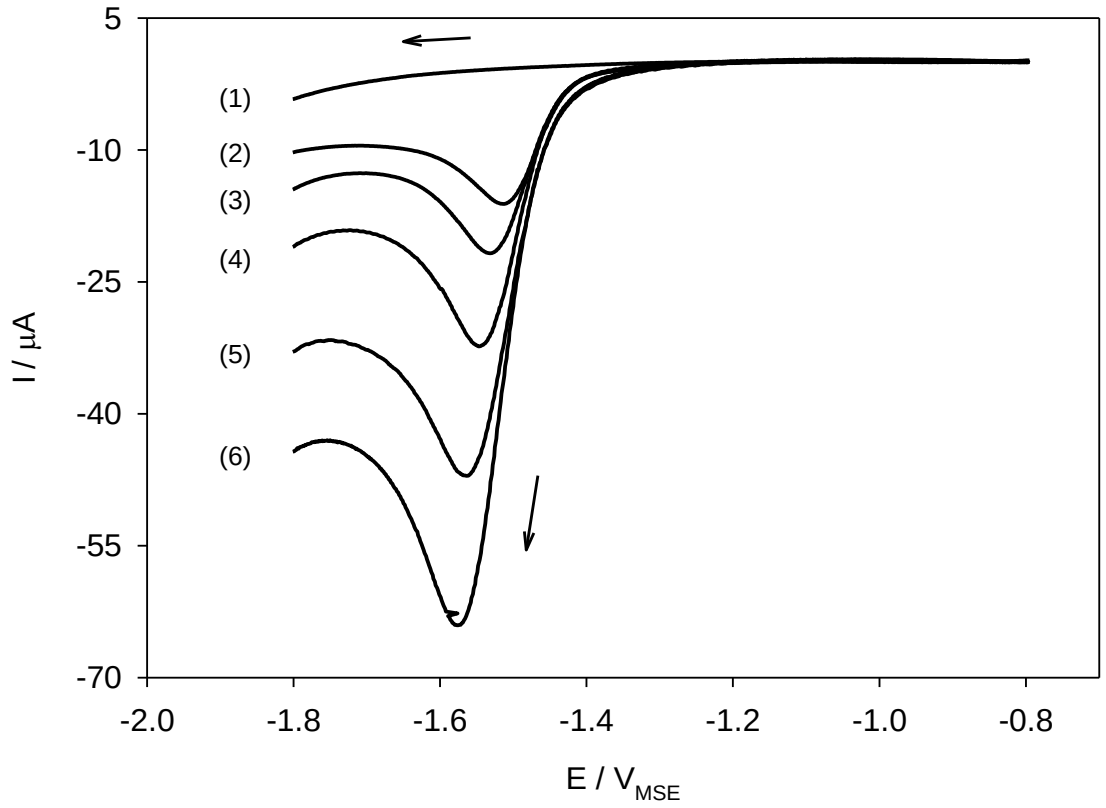

Figure 1. Linear voltammograms of NAD^+ reduction on GC electrode recorded in (1) the supporting electrolyte 0.1 M $NaClO_4$, and (2-6) in the supporting electrolyte containing 4 mM NAD^+. Scan rates: (1 and 2) 10, (3) 20, (4) 50, (5) 100 and (6) 200 mV s^{-1}. Temperature, T = 295 K.

However, the curves recorded in the NAD^+-containing electrolyte show a well-defined cathodic current peak at potentials negative of ca. –1.4 V. The peak is related to the NAD^+ reduction reaction (Scheme 1), and its potential is in agreement with the literature [3, 15, 18, 22, 24, 36, 39].

Fig. 1 indicates that the NAD^+ reduction reaction is irreversible in the potential region studied. Firstly, the potential difference between the first noticeable NAD^+ reduction current (around –1.3 V) and *formal potential* of the NAD^+/NADH couple, E' = –0.885 V (at pH 5.8) is rather high [22, 24, 25]. Secondly, no anodic peak in the returning (positive) cycle was observed even when the anodic limit was extended to 0 V (not shown). This high NAD^+ reduction overpotential is due to an unfavorable surface orientation of NAD^+ on the electrode surface [22, 23].

The peak position (potential) in Fig. 1 shifts towards more negative potentials with an increase in scan rate. This indicates that the NAD^+ reduction reaction is under mass-transport control. In order to verify this, the dependence between the peak current and square root of scan rate was plotted in Fig. 2. The graph shows a linear dependence, thus confirming that the reaction is indeed under mass-transport control under the experimental conditions applied [22, 24, 25, 40, 41].

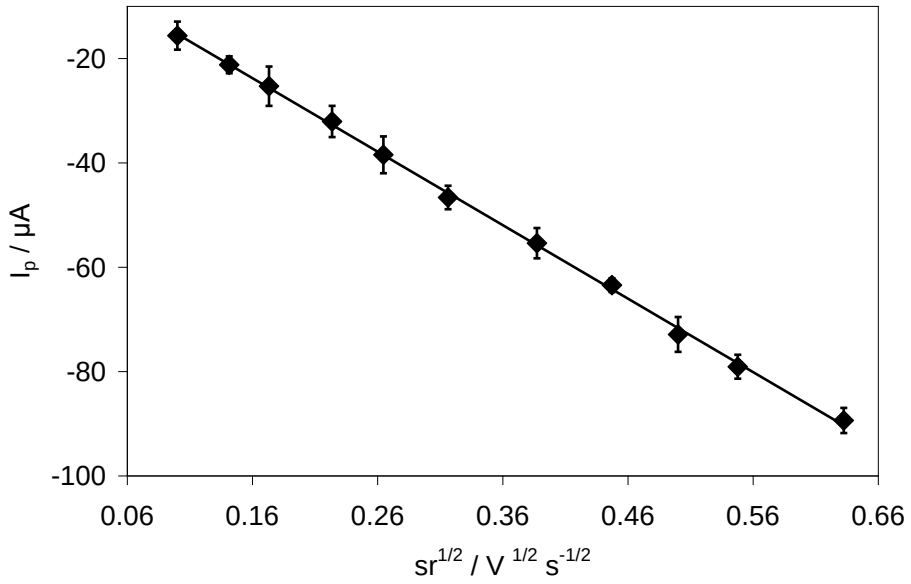

Figure 2. Dependence of NAD^+ reduction peak current on the applied scan rate obtained from the voltammograms presented in Fig. 1.

Next, a kinetic parameter, *αn*, related to the electron-transfer process was calculated. In this product, α represents the fraction of applied potential used to lower the activation energy for NAD^+ reduction (*i.e.* the transfer coefficient), while *n* represents a number of electrons exchanged in the NAD^+ reaction. In order to calculate the *αn* value from the data in Fig. 1, the peak potential versus logarithm of scan rate dependence was plotted in Fig. 3.

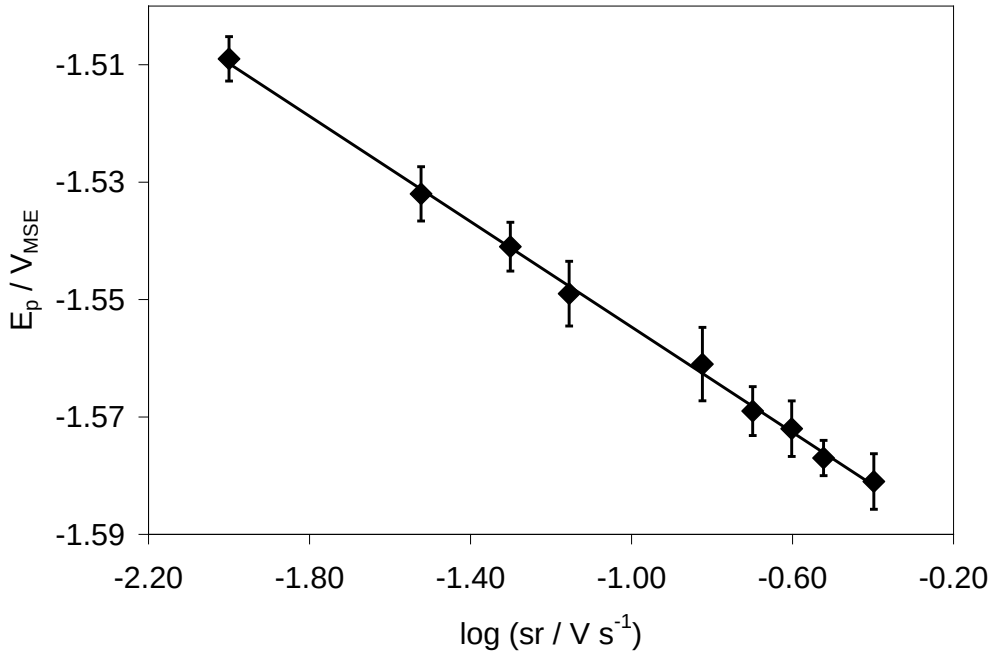

Figure 3. Dependence of NAD^+ reduction peak potential on the applied scan rate obtained from the voltammograms presented in Fig. 1.

Taking into account that the NAD^+ reduction reaction is irreversible, the following equation can be employed to evaluate the αn product [24, 25, 42-44]:

$$\frac{dE_p}{d\log(sr)} = \frac{-0.029}{\alpha n} \quad (1)$$

where E_p is the peak potential (V) and sr is the scan rate (V s^{-1}). Thus, taking the value of the slope in Fig. 3, the product was calculated to be $\alpha n = 0.69$. This value is consistent with previous studies on Hg, Au and Ru-GC electrodes [22, 24, 26].

It would now be interesting to calculate the actual number of electrons involved in the NAD^+ reduction reaction, since this could provide information on the relative amount of NAD_2 and NADH produced within the potential region of the LV peak in Fig. 1. This would provide information on the selectivity of the bare GC electrode in regenerating 1,4-NADH (as opposed to NAD_2) under the experimental conditions applied. For this purpose, the slop in Fig. 2 and the following equation can be used [22, 25, 43, 45, 46]:

$$I_p = 2.99\times10^5 nA(\alpha n)^{1/2}[NAD^+]D^{1/2}sr^{1/2} \quad (2)$$

where n is the number of electrons participating in the redox reaction, $[NAD^+]$ is the concentration of NAD^+ in the bulk solution (mol cm^{-3}), A is the area of electrode (cm^2), D is the NAD^+ diffusion coefficient in the solution (cm^2 s^{-1}) and sr is the potential scan rate (V s^{-1}). Taking that αn = 0.69, a value of n = 1.62 was calculated, and that of apparent transfer coefficient, α = 0.43. Taking that the NAD_2 formation requires one electron per one NAD^+ molecule, while the formation of 1,4-NADH requires the exchange of two electrons (Scheme 1), the number of electrons calculated from the LV curves in Fig. 1 (n = 1.62) indicates that 62% of 1,4-NADH was formed by the reduction of NAD^+ under potentiodynamic conditions in Fig. 1.

In order to verify the kinetic information obtained from Figs. 2 and 3, a set of LVs were recorded at a constant scan rate, but at varying NAD^+ concentrations, Fig. 4a. The plot shows that with an increase in NAD^+ concentration in the solution, the NAD^+ reduction peak current also increases, which is in agreement with Eq. (2). Indeed, the inset (Fig. 4b) demonstrates that this dependence is linear, as predicted by equation (2). Thus, taking the previously calculated value of the product αn = 0.69, it was possible to calculate the number of electrons exchanged in the NAD^+ reduction reaction and the corresponding transfer coefficient, n = 1.66 of α = 0.42, respectively. These values are very close to those calculated from LVs in Fig. 1.

In addition, since the peak current is proportional to the NAD^+ reduction rate, $d[NAD^+]/dt$, the linear dependence between the NAD^+ reduction peak current and NAD^+ concentration in the bulk solution, Fig. 4b, indicates that the NAD^+ reduction reaction is of pseudo-first order with respect to NAD^+, under the experimental conditions performed.

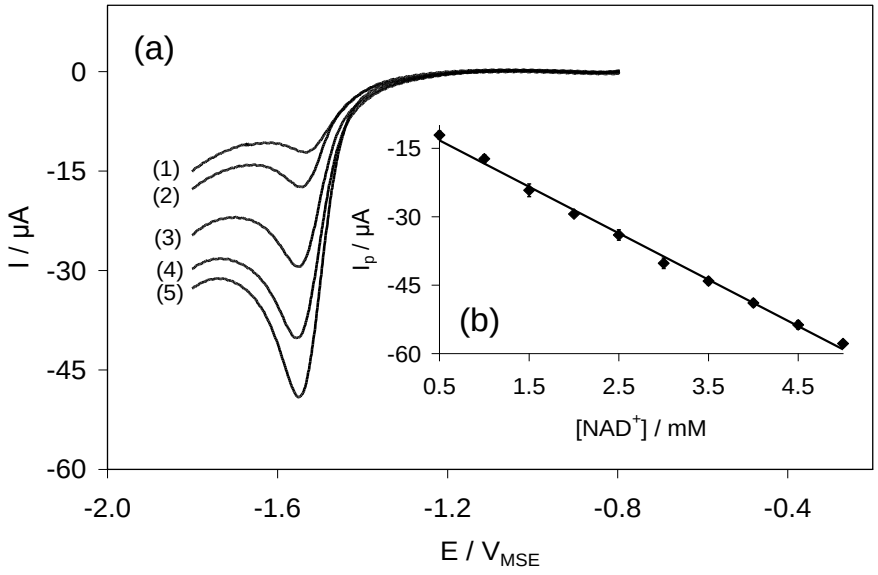

Figure 4. (a) Linear voltammograms of NAD^+ reduction on GC electrode recorded in 0.1 M $NaClO_4$ containing various concentrations of NAD^+: (1) 0.5 mM, (2) 1 mM, (3) 2 mM, (4) 3 mM and (5) 4 mM. Scan rate, sr = 100 mV s^{-1}; temperature, T = 295 K. (b) Dependence of the peak current on the NAD^+ concentration obtained from the data presented on the main plot (a).

3.2. Differential pulse voltammetry

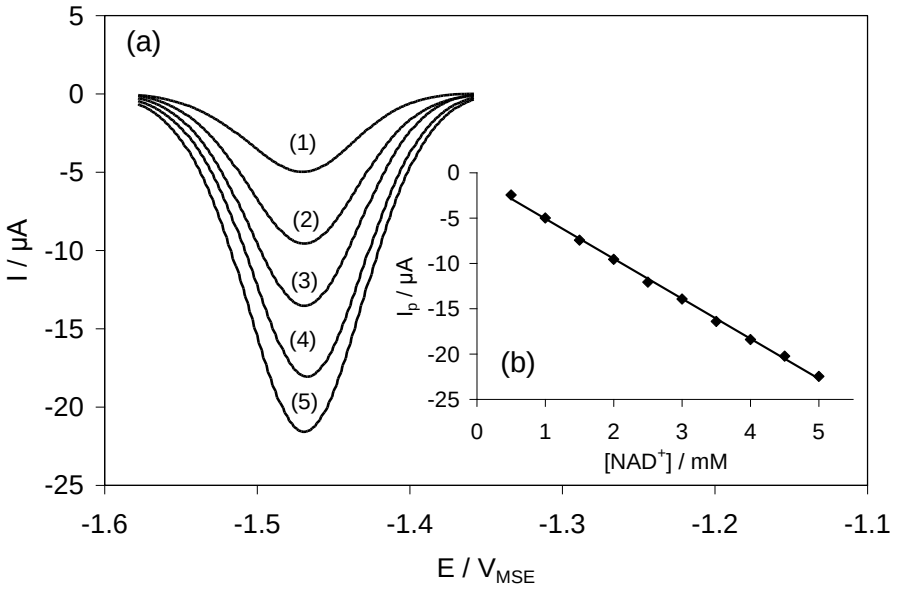

Figure 5. (a) Differential pulse voltammograms of NAD^+ reduction on GC electrode, recorded in 0.1 M $NaClO_4$ containing various concentrations of NAD^+: (1) 1 mM, (2) 2 mM, (3) 3 mM, (4) 4 mM and (5) 5 mM. Modulation time, 70 ms; modulation amplitude, 50 mV; interval time, 0.2 s; step potential, 1.5 mV; scan rate, sr = 7.5 mV s^{-1}; temperature, T = 295 K. (b) Dependence of the peak current on the NAD^+ concentration obtained from the data presented on the main plot (a).

DPV technique was chosen as an independent technique for the verification of the kinetic parameters calculated from LVs in Figs. 1 and 4. Fig. 5a shows a set of DPVs recorded at various concentrations of NAD^+ in the supporting electrolyte. With an increase in NAD^+ concentration, the DPV peak current increases in a linear manner, as demonstrated in the inset, Fig. 5b. The same as the corresponding behavior obtained in LV measurements presented in Fig. 4, the results in Fig. 5 also indicate that the NAD^+ reduction reaction on the bare GC electrode is of pseudo-first order with respect to NAD^+. Similar results were also obtained previously in our laboratory on Au [24], and ruthenium-modified GC electrodes [22].

The DPV results in Fig. 5 can also be used to calculate the product αn, by determining the width of the DPV peak at its half height, $W_{1/2}$ (V), at each NAD^+ concentration [25, 47]:

$$W_{1/2} = \frac{3.52RT}{\alpha nF} \tag{3}$$

where F is the Faraday constant (96485 C mol^{-1}), R is the standard gas constant (8.314 J mol^{-1} K^{-1}), and T is the temperature (K). A value αn = 0.97 was obtained. Now, using the following equation [25, 46]:

$$I_p = \frac{nAFD^{1/2}[NAD^+]}{\sqrt{\pi t_m}}\left(\frac{1-\sigma}{1+\sigma}\right) \tag{4}$$

where for an irreversible electrochemical reaction [25, 48]:

$$\sigma = \exp\left(\frac{\alpha nF\Delta E}{2RT}\right) \tag{5}$$

and were t_m represents modulation time (s) and ΔE is the modulation amplitude (V), a number of electrons involved in the NAD^+ reduction reaction performed under the experimental conditions in Fig. 5 was calculated to be n = 1.54. This indicates that ca. 54% of 1,4-NADH was formed by the reduction of NAD^+. A slightly lower number of electrons exchanged (and hence the percentage of 1,4-NADH regenerated) in comparison to the LV measurements in Figs. 1 and 4 is due to the fact that the DPV peak is located at more positive potentials (ca. -1.47 V) in comparison to LV peaks (Fig. 3). Namely, as it was demonstrated by our previous work [16], the percentage of 1,4-NADH regenerated is potential dependent, and at -1.4 V it was 32% and at -1.5 V it was 64%. Employing linear interpolation, the percentage of 1,4-NADH regenerated at -1.47 V would be ca. 54%, which agrees well with the value obtained from Fig. 5. Table 1 summarizes kinetic values calculated from LV and DPV measurements. For comparison, the table also lists the corresponding values obtained from long-term NADH regeneration experiments performed in a batch electrochemical reactor employing a GC electrode [16]. As evidenced, the obtained values agree very well, thus verifying the accuracy of the LV and DPV values and the methods employed to obtain them.

Table 1. Kinetic parameters for NAD^+ reduction on a GC electrode obtained from different experimental electrochemical techniques.

Technique	Type	n_{exp}	α_{exp}
LV	Scan dependent	1.62	0.43
	Concentration dependent	1.66	0.42
DPV		1.54	0.63
Enzymatic assay (-1.47 V)		1.54*	
Enzymatic assay (-1.50 V)		1.64	
Average value		1.62	0.49
Standard deviation		0.05	0.12

* This value was calculated by the interpolation, as described in the text.

3.3. Electron transfer-rate constant and activation energy

To calculate a value of apparent *formal* heterogeneous electron-transfer rate constant, k^f, the number of electrons, n, and the apparent transfer coefficient, α, LV and DPV voltammograms recorded at various scan rates and NAD^+ concentrations were fitted by a kinetic model for an irreversible electrochemical reaction using the Ecochemie General Purpose Electrochemical System software [49].

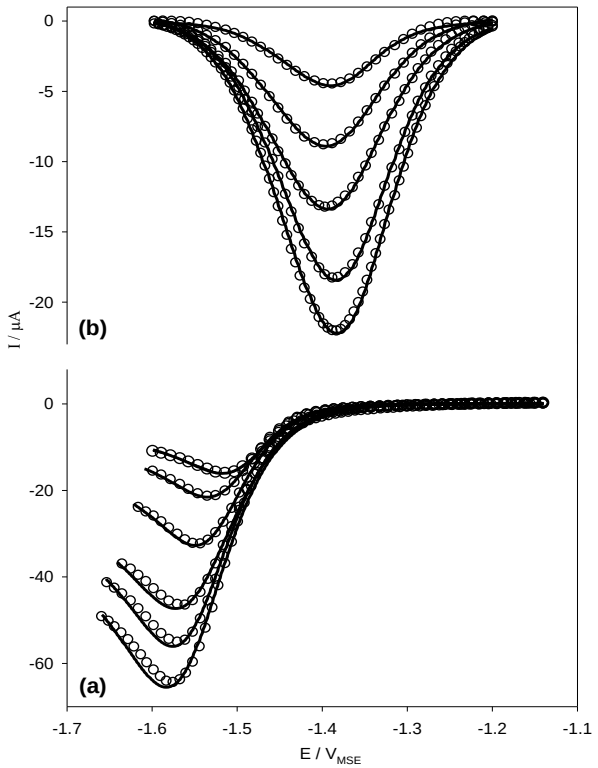

Figure 6. (a) Experimental (symbol) and simulated (line) LV voltammograms recorded at various scan rates in 0.1 M $NaClO_4$ + 4 mM NAD^+. The scan rate increases in the direction of the peak current increase as: 10, 20, 50, 100 and 200 mV s^{-1}. (b) Experimental (symbols) and simulated (line) DP voltammograms recorded in 0.1 M $NaClO_4$ containing various NAD^+ concentrations. The concentration increases in the direction of the peak increase as: 0.5, 1, 2, 3, and 4 mM. DPV experimental parameters are the same as those in Fig. 5. Temperature, T = 295 K.

Fig. 6 demonstrates that an excellent agreement between the simulated (solid line) and experimental (symbols) voltammograms was obtained. The mean value of the apparent formal heterogeneous electron-transfer rate constant calculated from scan- and concentration-dependent LV measurements is $k^f = (6.1 \pm 2) \times 10^{-14}$ cm s^{-1}. A close value was also obtained from concentration-dependent DPV measurements $k^f = (2.5 \pm 1) \times 10^{-14}$ cm s^{-1}. Previous studies on the Au electrode also yielded such low values [24]. These low values indicate very slow kinetics of the NAD^+ reduction reaction at the *formal potential* of the NAD^+/NADH couple (–0.885 V). This was expected considering the irreversibility / high overpotential of the NAD^+ reduction reaction on a GC electrode (Figs. 1, 4, 5 and 6).

The fitting of the LV and DPV curves also yielded an average value of the *αn* product, 0.79, which allowed for the calculation of the corresponding apparent transfer coefficient α = 0.5 and number of electrons involved in the reaction, *n* = 1.58. These values are in a very good agreement with the experimental values obtained by analyzing the LV and DPV peaks (Table 1).

LV and DPV techniques were also utilized to investigate the effect of temperature on the NAD^+ reduction kinetics, *i.e.* to calculate the corresponding activation energy.

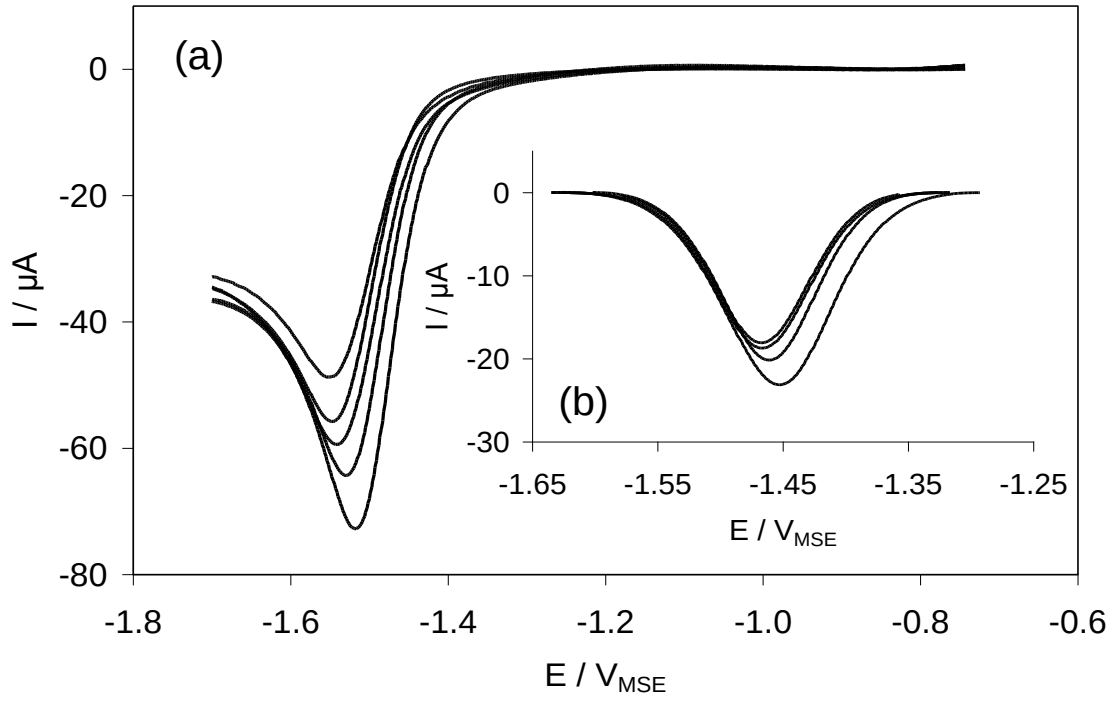

Figure 7. (a) LVs of GC electrode in 0.1 M $NaClO_4$ + 4 mM of NAD^+ solution recorded at various temperatures. The temperature increases in the direction of the peak increase as: 295, 304, 310, 315 and 325 K. Scan rate, 100 mV s^{-1}. (b) Differential pulse voltammograms of NAD^+ reduction on GC electrode recorded in 0.1 M $NaClO_4$ + 4 mM of NAD^+. The temperature increases in the direction of the peak increase as: 295, 304, 315 and 325 K. DPV experimental parameters are the same as those in Fig. 5.

Fig. 7 shows LVs and DPVs obtained at selected temperatures and at a constant NAD^+ concentration in the bulk solution. The peak current increases with the increase in temperature, indicating that the kinetics of NAD^+ reduction also increases. To calculate the corresponding activation energy, a set of LVs and DPVs were recorded at a constant temperature and various NAD^+ concentrations (for example, see Figs. 4 and 5). Then, the dependence of peak current, I_p, on NAD^+ concentration was analyzed, as in Figs. 4 and 5. In all cases, a linear dependence was obtained, confirming that the NAD^+ reaction is of pseudo-first order with respect to NAD^+ in the temperature range investigated:

$$I_p = k_{eff}\left[NAD^+\right] \tag{6}$$

where k_{eff} is effective NAD^+ reduction reaction rate constant (A cm^3mol^{-1}).

Now, the dependence of the effective rate constant on temperature is analyzed in accordance with the Arrhenius law:

$$k_{eff} = A\exp\left(\frac{-\Delta G_{act}}{RT}\right) \tag{7}$$

where A is pre-exponential factor (A cm^3 mol^{-1}), ΔG_{act} is the Gibbs energy of activation (J mol^{-1}), and the remaining quantities have already been defined previously.

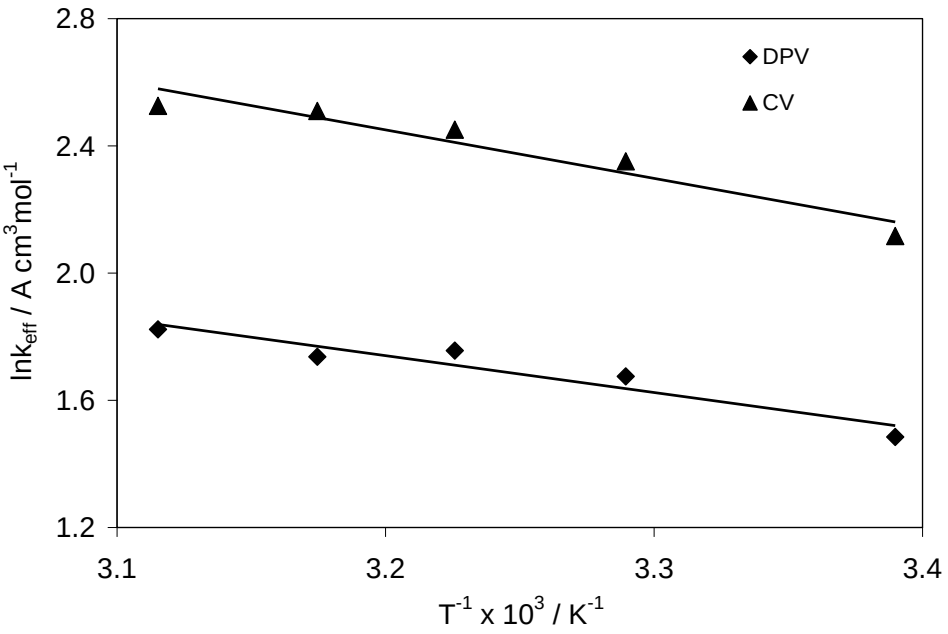

Figure 8. Dependence of effective rate constant on temperature obtained from LV and DPV measurements recorded on GC electrode in 0.1 M $NaClO_4$ containing various NAD^+ concentrations. (LV) scan rate, 100 mV s^{-1}. (DPV) modulation time, 70 ms; modulation amplitude, 50 mV; interval time, 0.2 s; step potential, 1.5 mV; scan rate, sr = 7.5 mV s^{-1}.

Fig. 8 shows the resulting behavior. The behavior is linear, as expected from the Arrhenius law. From the slope of the lines, apparent Gibbs energy of activation values for the reduction of NAD^+ on the bare GC electrode were calculated for the reaction occurring in the potential region of LV and DPV peaks, $\Delta G_{act,LV}$ = 12.7 kJ mol^{-1} and $\Delta G_{act,DPV}$ = 12.1 kJ mol^{-1}, respectively. However, it is more convenient to report ΔG_{act} at *formal* potential because Gibbs energy of activation is potential dependent according to the following equation [24, 40]:

$$\Delta G_{act,formal} = \Delta G_{act,peak} - \alpha n F \eta \quad (8)$$

where η represents the overpotential (V). Taking the average value of the αn product (αn = 0.69), the apparent formal Gibbs energy of activation value at formal potential of the NAD^+/NADH redox couple was calculated to be $\Delta G_{act,LV}$ = 53.6 kJ mol^{-1} (LV measurements) and $\Delta G_{act,DPV}$ = 53.1 kJ mol^{-1} (DPV measurements). Therefore, the two different experimental techniques gave values that agree very well, thus confirming their reliability. Similar values were reported in the literature using Ru-GC [22] and Au electrodes [24]. Based on the apparent formal activation energy values obtained, it appears that the reduction of NAD^+ on GC is only a moderately temperature dependent reaction.

3.4. Electrochemical impedance spectroscopy

EIS was implemented to get more information on the GC electrode/electrolyte interface in the presence of NAD^+, and on the NAD^+ reduction kinetics. EIS studies were carried out with the same setup that was used for potentiodynamic polarization studies. The applied *ac* perturbation signal was ±10 mV within the frequency range from 50 kHz to 20 mHz.

3.4.1. Potential-dependent impedance measurements

EIS data of the GC electrode recorded at several potentials in the double-layer and NAD^+ reduction region are presented in Fig. 9, in a form of Nyquist plots. Figs. 9b and 9c display the response of the GC electrode in the presence (circles) and absence (triangles) of NAD^+ in the supporting electrolyte. At –0.9 V (Fig. 9b), which is in the potential region more positive of the NAD^+ reduction peak in Fig. 1, the two spectra overlap, confirming that the NAD^+ reduction does not occur at this potential. However, at –1.1 V (Fig. 9c) the spectrum recorded in the presence of NAD^+ (circles) displays a smaller-diameter quarter-circle than that in the absence of NAD^+ (triangles), indicating the occurrence of the NAD^+ reduction reaction [24]. If we compare this to the results obtained using LV and DPV, we can see that the onset of NAD^+ reduction in the *dc* measurements can be noticed only at potentials negative of ca. –1.25 V. This confirms that EIS is a more sensitive technique for the detection of reactions kinetics than the two *dc* techniques.

Further, if the electrode potential is biased to values negative of –1.1 V, the diameter of the EIS semicircle further decreases (Fig. 9a), indicating an increase in the NAD^+ reduction kinetics [23]. This is in accordance with the results obtained by LV and DPV measurements.

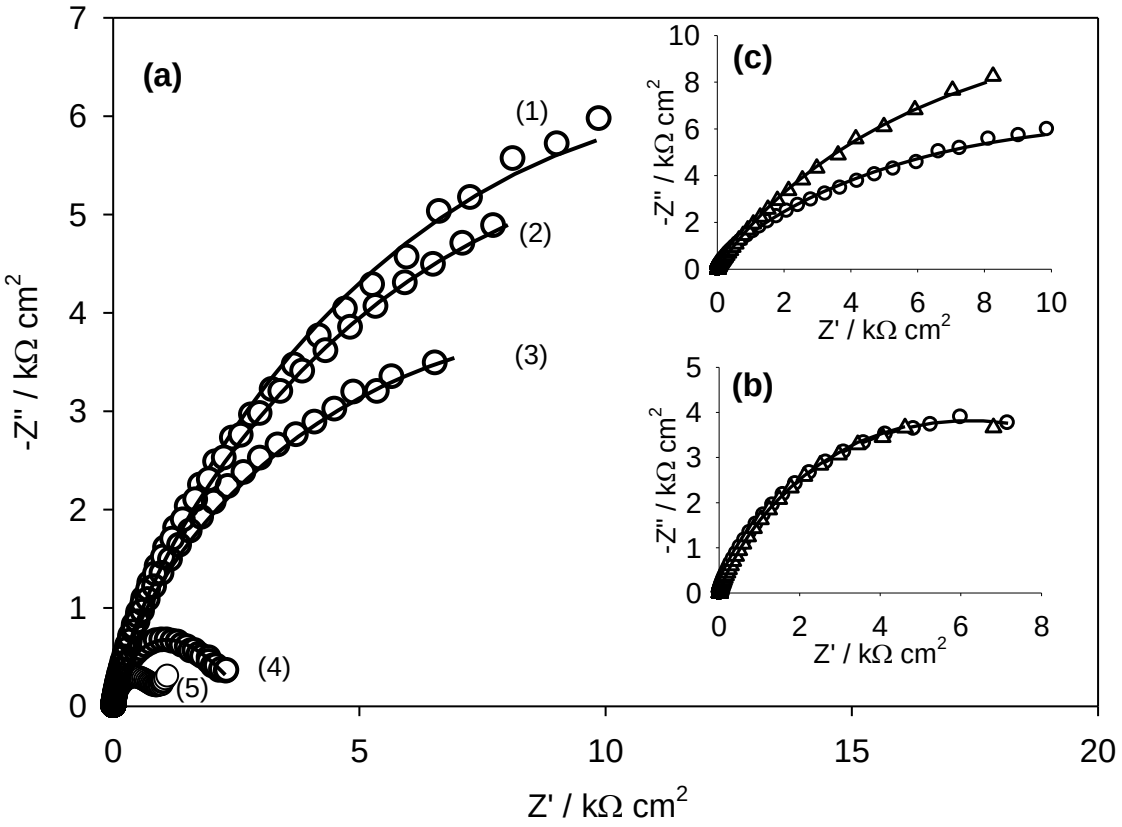

Figure 9. (a) Nyquist plot of a GC electrode recorded at various *dc* potentials (1) −1.1 V (2) –1.2 V (3) –1.3 V (4) –1.4 V and (5) –1.45 V in 0.1 M $NaClO_4$ + 4 mM NAD^+. (b) Nyquist plots of a GC electrode at (b) –0.9 V and (c) –1.1 V in (Δ) 0.1 M $NaClO_4$ and (O) 0.1 M $NaClO_4$ + 4 mM NAD^+. The solid lines represent the simulated spectra obtained using the equivalent electrical circuit model presented in Fig. 10. Temperature, T = 295 K.

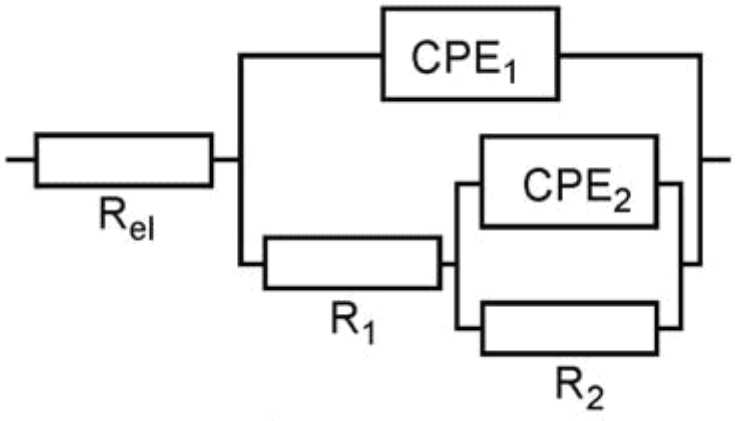

Figure 10. Electrical equivalent circuit used to model the EIS data. R_{el} represents electrolyte resistance between the working and reference electrode, while the meaning of other elements is explained in the text.

To quantify the EIS results, the experimental spectra in Fig. 9 were modeled using non-linear least-squares fit analysis (NLLS) software [50] and an electrical equivalent circuit (EEC) presented in Fig. 10. The modeled data are presented as solid lines in Fig. 9. It is evident that the agreement between the experimental data (symbols) and modeled data (lines) is very good, confirming the validity of the proposed EEC in describing the impedance behavior of the investigated system under the given experimental conditions.

The proposed EEC model is comprised of two time constants; the high-frequency (HF) time constant, τ_1 ($\tau_1 = \mathrm{CPE}_1 R_1$), and the low frequency (LF) time constant, τ_2 ($\tau_2 = \mathrm{CPE}_2 R_2$). This circuit models a response where polarization is due to a combination of kinetic and diffusion processes. Here R (Ω) stands for the resistance and CPE (Ω^{-1} s^n) for the constant phase element. The impedance of the latter is defined as $Z_{CPE} = [\mathrm{CPE}(j\omega)^n]^{-1}$,

where ω (rad s^{-1}) represents the radial frequency. If n = 1, Z_{CPE} behaves as a perfect capacitance, while n = 0 represents a perfect resistance and if n = 0.5 it acts like a Warburg (mass transport) impedance [51]. Values of n other than the ideal values mentioned above indicate the presence of heterogeneities such as surface roughness, and/or adsorbed species [52, 53].

The modeling of the EIS spectra in Fig. 9 resulted in a value of the constant phase element (CPE_1) exponent $n_1 = 0.87 \pm 0.02$. Hence, CPE_1 represents a response of a capacitor, in this case a response of the electrochemical double-layer capacitance. The corresponding parallel resistance R_1 (Fig. 10) is the charge transfer resistance or polarization resistance (depending on the potential).

The second EEC branch (Fig. 10) is composed of CPE_2 and R_2. CPE_2 is located in the LF domain of the spectrum, and the fitting of the spectra in Fig. 9 gave a mean value of its exponent $n_2 = 0.52 \pm 0.03$. As this value is close to 0.5, it indicates a response of a diffusion-controlled process. Hence this capacitance is related to the diffusive pseudo-capacitance (or Warburg impedance, W) and R_2 is the corresponding resistance to mass transfer. Besides the diffusive response related to mass transport of NAD^+ towards the electrode surface, traces of phenolic and carboxylic functional groups commonly found on the GC surface could also contribute to diffusive capacitance [54].

In the EEC in Fig. 10, the sum of charge transfer resistance (R_1) and mass-transport resistance (R_2) represents the total resistance (R_T) related to the kinetics of the parallel NAD^+ reduction and hydrogen evolution reaction. Its inverse value, R_T^{-1}, could thus be related to the total *dc* current measured under the potentiostatic conditions, $1/I$ [24]. The dependence of R_T^{-1} on the applied *dc* potential obtained from the EIS data recorded in the supporting electrolyte (triangles) and NAD^+-containing solution (circles) is shown in Fig. 11a.

The data obtained in the absence of NAD^+ in the supporting electrolyte (triangles) is relatively constant, while in the presence of NAD^+ (circles) the R_T^{-1} value starts increasing at potentials negative of –1.2 V, which is due to the reduction of NAD^+ on the electrode surface (note that the EIS spectra in Fig. 9c shows that NAD^+ is being reduced already at –1.1 V, but the large scale of the ordinate in Fig. 11 prevents the visual distinction between the two responses at potentials positive of –1.2 V). In conclusion, the NAD^+ reduction EIS data (Fig. 11) are in agreement with the LV data (Fig. 1), thus validating the NAD^+ reduction behavior recorded and the experimental approaches used in investigating the kinetics of NAD^+ reduction on the GC electrode, under the experimental conditions applied.

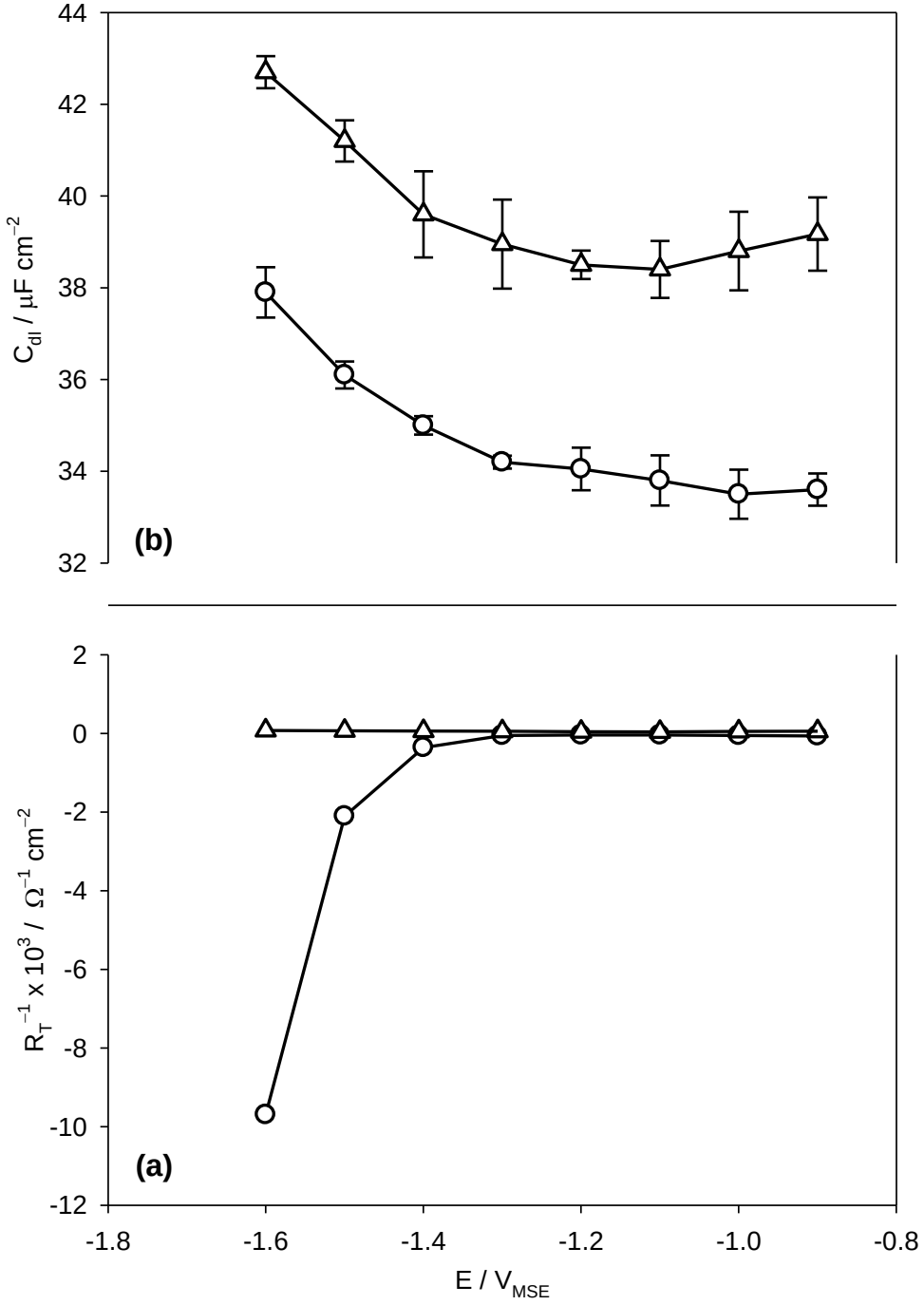

Figure 11. Dependence of the (a) inverse of total resistance and (b) double-layer capacitance on the applied *dc* potential obtained by fitting the EIS spectra in Fig. 9a. (Δ) 0.1 M $NaClO_4$ and (O) 0.1 M $NaClO_4$ + 4 mM NAD^+. In (a) negative sign of the ordinate is used only to emphasize the cathodic character of NAD^+ reduction reaction. Error bars in Fig. 11a are not visible since the largest error is 0.015×10^{-3} $\Omega^{-1}cm^{-2}$.

Reduction of NAD^+ on the GC electrode surface might involve adsorption of either NAD^+ or the corresponding reduction reaction products, NADH and/or NAD_2 [24]. Thus, if the electrode

surface gets covered by an adsorbed molecular layer formed during the NAD^+ reduction reaction, and if this layer is stable on the electrode surface, the EIS spectra should detect such a response. More particularly, if there is a blockage of the electrode surface by adsorbents that have a lower dielectric constant than water, then there should be a decrease in the electrochemical double-layer capacitance, according to the electrochemical double-layer theory [55]. To investigate this, the behavior of the electrochemical double-layer capacitance (CPE_1) obtained in EIS experiments presented in Fig. 9 was further analyzed. A true value of the double-layer capacitance was calculated using the equation proposed by Brug *et al.* [56]:

$$C_{dl} = [CPE_1(R_{el}^{-1} + R_1^{-1})^{n_1 - 1}]^{1/n_1} \quad (9)$$

The results are plotted in Fig. 11b. The plot shows the potential-dependent behavior of the double-layer capacitance in the absence (triangles) and presence (circles) of NAD^+ in the solution. The double-layer capacitance of the NAD^+-containing solution is lower than that obtained in the absence of NAD^+, in the whole potential region studied. This confirms that NAD^+ indeed adsorbs on the GC surface in the potential region presented in the figure, and this region covers both the region where NAD^+ is not reduced (positive of –1.1 V, *i.e.* the electrochemical double-layer region) and the region where NAD^+ undergoes reduction (negative of –1.1 V). However, one cannot exclude a possible adsorption of NAD_2 and NADH formed in the NAD^+ reduction reaction at potentials negative of 1.1 V.

3.4.2. Concentration-dependent impedance measurements

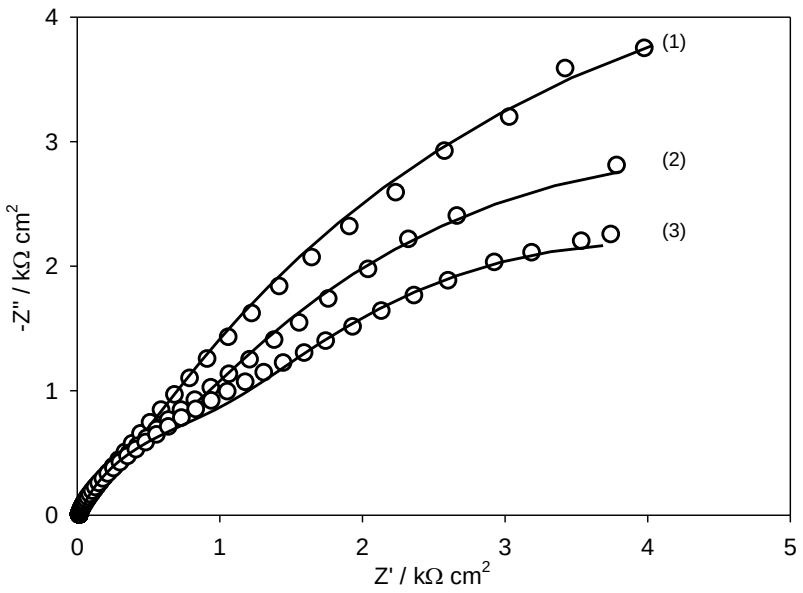

Figure 12. Nyquist plot of a GC electrode recorded at various concentrations of NAD^+ in 0.1 M $NaClO_4$: (1) 0.5 mM, (2) 2 mM, and (3) 3 mM. Applied *dc* potential, E_{dc} = -1.5 V_{MSE}; temperature, T = 295 K.

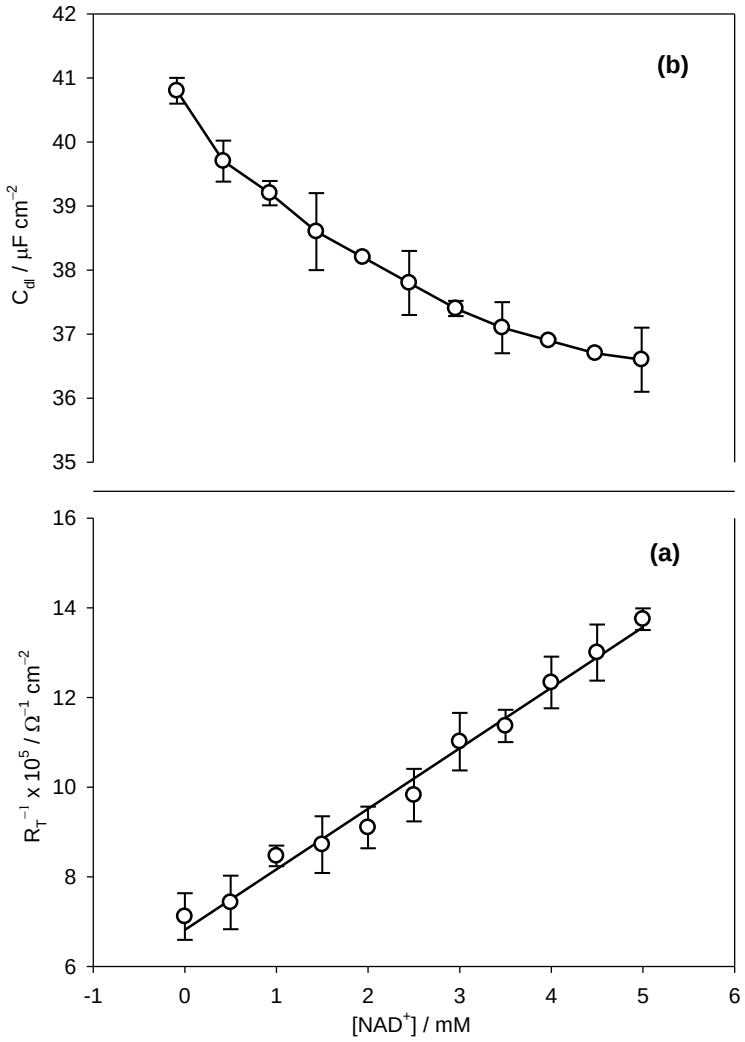

Figure 13. Dependence of the (a) inverse of total resistance and (b) double-layer capacitance on the NAD^+ concentration obtained by fitting the EIS spectra in Fig. 12.

Concentration-dependent EIS behavior was also studied in the potential region of NAD^+ reduction, and selected spectra are shown in Fig. 12. The spectra clearly show the appearance of two semicircles confirming the presence of two time constants, namely the high-frequency (HF) time constant, τ_1, and the low frequency (LF) time constant, τ_2 (Fig. 10), which could be explained in the same manner as those in the previous section of the manuscript (Section 3.4.1).

As the concentration of NAD^+ in solution increases, the total resistance (R_T) to the NAD^+ reduction reaction decreases, while the corresponding inverse value, R_T^{-1}, increases linearly, as shown in Fig. 13a. Knowing that current is proportional to inverse resistance ($I \propto R^{-1}$); the linear trend in Fig. 13a indicates that the NAD^+ reduction reaction is of pseudo-first order with respect to NAD^+. Although the EIS measurements in Fig. 13 were preformed potentiostatically, the trend in the figure is very similar to that obtained from linear polarization measurements presented in Fig. 4b, *i.e.* in both cases the reaction was found to be of pseudo-first order with respect to NAD^+.

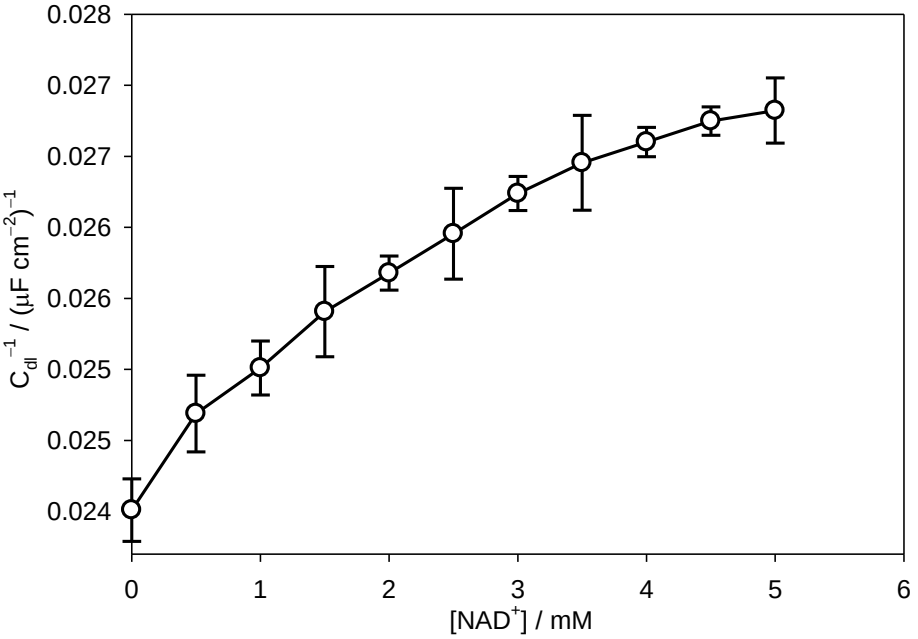

Figure 14. Inverse of double-layer capacitance as a function of NAD^+ concentration obtained from Fig. 13b.

Further, it would also be of interest to examine the behavior of the electrochemical double-layer capacitor, CPE_1 (*i.e.* C_{dl}) with NAD^+ concentration. For this purpose, C_{dl} values were calculated at each NAD^+ concentration using Eq. (9), and the resulting values are presented in Fig. 13b. The trend in the figure demonstrates that with an increase in NAD^+ concentration in the bulk solution, the double-layer capacitance decreases. This indicates that the electrode surface coverage by adsorbed NAD^+ (and/or NADH and/or NAD_2) increases with NAD^+ concentration in the bulk solution, displaying an adsorption-type behavior. The latter is more evident from Fig. 14, which represents the inverse of Fig. 13b, and displays a behavior of a classical adsorption isotherm.

4. CONCLUSIONS

Interaction of NAD^+ with a glassy carbon (GC) electrode surface, in term of the NAD^+ reduction kinetics was investigated at various temperatures (295 to 331 K), electrode potentials (–1.1 to –1.5 V) and NAD^+ concentrations (1 to 5 mM) using electrochemical methods of linear polarization voltammetry, differential pulse voltammetry and electrochemical impedance spectroscopy. A very good agreement among results produced by the three techniques was demonstrated. The NAD^+ reduction on GC under the potentiodynamic polarization conditions in the potential region of LV and DPV current peaks results in the formation of ca. 54 to 62 mol % 1,4-NADH. It was found that the NAD^+ reduction reaction is under diffusion control, is irreversible (requires overpotential of more than -550 mV), and is of pseudo-first order with respect to NAD^+. The kinetics of reduction of NAD^+ on GC at a *formal* potential of the NAD^+/NADH couple (-0.885 V) was found to be rather slow and

moderately temperature dependent: the apparent formal heterogeneous electron-transfer rate constant is in the order of 10^{-14} cm s^{-1}, and the apparent formal Gibbs energy of activation is ca. 53.1 kJ mol^{-1}.

ACKNOWLEDGEMENTS
The authors would like to acknowledge the Natural Science and Engineering Research Council of Canada and the University of Engineering and Technology, Peshawar, Pakistan for providing the support for this research.

Nomenclature

A	pre-exponential factor in the Arrhenius equation (A cm^3 mol^{-1})
[-]	concentration (mol cm^{-3}) or (mM or mol L^{-1})
C_{dl}	double-layer capacitance (F cm^{-2})
CPE	constant phase element (Ω^{-1} s^n cm^{-2})
D	diffusion coefficient (cm^2 s^{-1})
E'	formal potential (V)
E_p	peak potential (V)
ΔE	modulation amplitude (V)
F	Faraday constant (96,485 C mol^{-1})
ΔG_{act}	apparent Gibbs energy of activation (kJ mol^{-1})
$\Delta G_{act,LV}$	apparent Gibbs energy of activation determined at a LV peak potential (kJ mol^{-1})
$\Delta G_{act,DPV}$	apparent Gibbs energy of activation determined at a DPV peak potential (kJ mol^{-1})
I_p	peak current (A)
k_{eff}	effective heterogeneous electron-transfer rate constant (A cm^3 mol^{-1})
k^f	apparent formal heterogeneous electron-transfer rate constant (cm s^{-1})
n	number of electrons
n	exponent of a constant phase element
R	standard gas constant (8.314 J mol^{-1} K^{-1})
R	resistance (Ω cm^2)
sr	scan rate (V s^{-1})
t_m	modulation time (s)
T	temperature (K)
W	Warburg impedance element (Ω^{-1} $s^{1/2}$ cm^{-2})
$W_{1/2}$	width of a DPV peak (at half height) (V)
Z	impedance (Ω cm^2)

Greek letters

α	transfer coefficient
η	overpotential (V)
τ	time constant (s)
ω	radial frequency (rad s^{-1})

References

1. A. Schmid, J.S. Dordick, B. Hauer, A. Kiener, M. Wubbolts, B. Witholt, *Nature*, 409 (2001) 258.
2. A. Liese, K. Seelbach, C. Wandrey, *Industrial Biotransformations*, Wiley-VCH, Weinheim (2006).
3. Y.H. Kim, Y.J. Yoo, *Enzyme. Microb. Technol*., 44 (2009) 129.

4. F. Pariente, F. Tobalina, M. Darder, E. Lorenzo, H.D. Abruna, *Anal. Chem*., 68 (1996) 3135.
5. R. Devaux-Basseguy, A. Bergel, M. Comtat, *Enzyme. Microb. Technol*., 20 (1997) 248.
6. R.A. van Santen, P.W.N.M. van Leeuwen, J.A. Moulijn, B.A. Averill, *Catalysis: An Integrated Approach*, Elsevier, Amsterdam (1999).
7. A. Rongvaux, F. Andris, F. Van Gool, O. Leo, *BioEssays*, 25 (2003) 683.
8. K. Delecouls-Servat, A. Bergel, R. Basseguy, *Bioprocess Biosyst. Eng*., 26 (2004) 205.
9. P. Belenky, K.L. Bogan, C. Brenner, *Trends Biochem. Sci*., 32 (2007) 12.
10. A.C. Pereira, M.R. Aguiar, A. Kisner, D.V. Macedo, L.T. Kubota, *Sens. Actuators*, B, 124 (2007) 269.
11. N. Pollak, C. Dolle, M. Ziegler, *Biochem. J.*, 402 (2007) 205.
12. A.A. Sauve, *J. Pharmacol. Exp. Ther*., 324 (2008) 883.
13. http://www.sigmaaldrich.com
14. H.K. Chenault, G.M. Whitesides, *Appl. Biochem. Biotechnol.*, 14 (1987) 147.
15. S.H. Baik, C. Kang, I.C. Jeon, S.E. Yun, *Biotechnol. Tech.*, 13 (1999) 1.
16. I. Ali, B. Soomro, S. Omanovic, *Electrochem. Commun*., 13 (2011) 562.
17. I. Ali, A. Gill, S. Omanovic, *Chem. Eng. J.*, 188 (2012) 173.
18. G. Rahman, J.Y. Lim, K.D. Jung, O.S. Joo, *Electrochem. Commun*., 12 (2010) 1371.
19. A. Salimi, M. Izadi, R. Hallaj, S. Soltanian, H. Hadadzadeh, *J. Solid State Electrochem.*, 13 (2009) 485.
20. E. Siu, K. Won, B.P. Chan, *Biotechnol. Prog.*, 23 (2007) 293.
21. Y.T. Long, H.Y. Chen, *J. Electroanal. Chem*., 440 (1997) 239.
22. A. Azem, F. Man, S. Omanovic, *J. Mol. Catal. A: Chem*., 219 (2004) 283.
23. A. Damian, K. Maloo, S. Omanovic, *Chem. Biochem. Eng*. Q., 21 (2007) 21.
24. A. Damian, S. Omanovic, *J. Mol. Catal. A: Chem*., 253 (2006) 222.
25. F. Man, S. Omanovic, *J. Electroanal. Chem*., 568 (2004) 301.
26. J.N. Burnett, A.L. Underwood, *Biochemistry*, 4 (1965) 2060.
27. C.O. Schmakel, K.S.V. Santhanam, P.J. Elving, *J. Am. Chem. Soc*., 97 (1975) 5083.
28. C.O. Schmakel, M.A. Jensen, P.J. Elving, *Bioelectrochem. Bioenerg*., 5 (1978) 625.
29. W.T. Bresnahan, J. Moiroux, Z. Samec, P.J. Elving, *Bioelectrochem. Bioenerg.*, 7 (1980) 125.
30. W.T. Bresnahan, P.J. Elving, *JACS.*, 103 (1981) 2379.
31. H. Jaegfeldt, *Bioelectrochem. Bioenerg*., 8 (1981) 355.
32. P.J. Elving, W.T. Bresnahan, J. Moiroux, Z. Samec, *Bioelectrochem. Bioenerg*., 9 (1982) 365.
33. M.A. Jensen, W.T. Bresnahan, P.J. Elving, *Bioelectrochem. Bioenerg*., 11 (1983) 299.
34. J. Moiroux, S. Deycard, T. Malinski, *J. Electroanal. Chem*., 194 (1985) 99.
35. M. Studnickova, H. Paulova-Klukanov, J. Turanek, J. Kovar, *J. Electroanal. Chem*., 252 (1988) 383.
36. J. Moiroux, P.J. Elving, *J. Electroanal. Chem*., 102 (1979) 93.
37. O.M.S. Filipe, C.M.A. Brett, *Electroanal.*, 16 (2004) 994.
38. S. Hrapovic, Y. Liu, K.B. Male, J.H.T. Luong, *Anal. Chem.*, 76 (2004) 1083.
39. Y. Nakamura, S.I. Suye, J.I. Kira, H. Tera, I. Tabata, M. Senda, *Biochim. Biophys. Acta - General Subjects*, 1289 (1996) 221.
40. A.J. Bard, L.R. Faulkner, *Electrochemical Methods: Fundamentals and Applications*, Wiley, (2001).
41. S. Sampath, O. Lev, *J. Electroanal. Chem*., 446 (1998) 57.
42. S.B. Saidman, E.C. Bellocq, J.B. Bessone, *Electrochim. Acta*, 35 (1990) 329.
43. S.E. Group, *Instrumental Methods in Electrochemistry*, Wiley, New York, (1985).
44. R.S. Nicholson, I. Shain, *Anal. Chem.*, 36 (1964) 706.
45. W.S. Kim, W.J. Sim, K.I. Chung, Y.E. Sung, Y.K. Choi, *J. Power Sources*, 112 (2002) 76.
46. J. Wang, *Analytical Electrochemistry*, Wiley, VCH, Massachusetts (2000).
47. P. Mericam, M. Astruc, X. Andrieu, *J. Electroanal. Chem*., 169 (1984) 207.

48. T.E. Edmonds, *Anal. Chim. Acta,* 116 (1980) 323.
49. Eco Chemie B.V., *General Purpose Electrochemical system,* Version 4.9.5.
50. B.A. Boukamp, *Equivalent Circuit Users Manual, Report CT88/265/128,* University of Twente, Department of Chemical Technology, The Netherlands, 1989.
51. H. Xiaoqiu, N. Duc, D.W. Greve, M.M. Domach, *IEEE, Sens. J.*, 4 (2004) 576.
52. S. Omanovic, S.G. Roscoe, *J. Colloid Interface Sci*., 227 (2000) 452.
53. S. Omanovic, S.G. Roscoe, *Langmuir,* 15 (1999) 8315.
54. K. Conway, *The Electrochemical Double Layer,* The Electrochemical Society, Inc, New Jersey, (1997).
55. G.Prentice, *Electrochemical Engineering Principles,* Prentice Hall, Upper Saddle River, New Jersey, (1991).
56. G.J. Brug, A.L.G. Van Den Eeden, M. Sluyters-Rehbach, J.H. Sluyters, *J. Electroanal. Chem*., 176 (1984) 275.